ACS Sustainable Chemistry & Engineering

Research Article

pubs.acs.org/journal/ascecg

Transition Metal-Doped Polyaniline/Single-Walled Carbon Nanotubes Nanocomposites: Efficient Electrode Material for High Performance Supercapacitors

Saptarshi Dhibar, Pallab Bhattacharya, Goutam Hatui, Sumanta Sahoo, and C. K. Das*

Materials Science Centre, Indian Institute of Technology Kharagpur, Kharagpur 721302, India

ABSTRACT: The demand for superior energy storage devices, such as supercapacitors, has been growing to meet the application requirements of hybrid vehicles and renewable energy systems. Here, we report a simple method to synthesize manganese chloride ($MnCl_2$)-doped polyaniline (PANI)/single-walled carbon nanotubes (SWCNTs) nanocomposites for electrochemical supercapacitors. The possible interactions between $MnCl_2$ and both PANI and SWCNTs was studied by Fourier transform infrared spectroscopy (FTIR), UV−visible spectroscopy, and Raman spectroscopy. The morphological characteristics of the electrode materials were investigated by field emission scanning microscopy (FESEM) and transmission electron microscopy (TEM). As-prepared nanocomposites showed higher electrical conductivity of 9.65 S/cm at room temperature and reached nonlinear current−voltage characteristics. A maximum specific capacitance of 546 F/g has been obtained for the nanocomposites at 0.5 A/g current density. Transition metal doping and SWCNTs enhance the electrochemical properties of the nanocomposites. The better specific capacitance and charge/discharge rates make them promising candidates as electrodes in supercapacitors, combining high energy densities with high levels of power delivery.

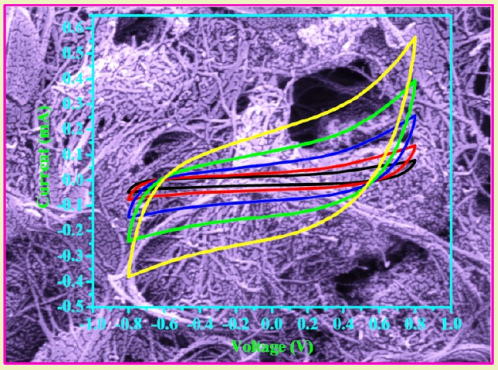

KEYWORDS: *Transition metal, Polyaniline, SWCNTs, Supercapacitors*

INTRODUCTION

With the rising concerns regarding global warming and the crisis of fuel, there has been a growing demand for sustainable energy based on renewable high efficiency energy conversions and storage technologies. Supercapacitors, one of the most promising electrochemical energy storage systems, have attracted much attention because of their pulse power supply, high dynamic of charge propagation, and long cycle life.[1,2] Supercapacitors can be used either by themselves as the primary power source or in combination with fuel cells or batteries. They show such high power density that they can complement the insufficiency of rechargeable batteries in the energy storage field. On the basis of the energy storage mechanism, they can be classified into two categories: electrochemical double-layer capacitors (EDLCs) and pseudocapacitors.

Conducting polymers (CP) such as polyaniline (PANI) have been regarded as electrode material in supercapacitors because of their easy synthesis, high controllable conductivity, good environmental stability, and simple acid/base doping/dedoping chemistry.[3,4] In recent years, PANI doped with various transition metal ions has attracted more research interest due to its potential applications as a redox-active catalyst,[5] corrosion inhibitor,[6] etc. When conducting polymers are doped with transition metal ions, for example, Cu^{2+}, Zn^{2+}, Fe^{2+}, and Co^{2+}, the dopants serve as redox active catalysts and enhance the capacitance and thus increase the energy density. There are mainly two types of carbon nanotubes (CNTs) that take part in the electrochemical capacitor: (i) single-walled carbon nanotubes (SWCNTs) and (ii) multi-walled carbon nanotubes (MWCNTs). Both types of nanotubes have high conductivity, but the use of SWCNTs is more beneficial as compared to MWCNTs in supercapacitor applications. This is mainly because of the higher conductivity, higher surface area, and interconnectivity of SWCNTs, and these properties are more crucial for getting better specific capacitance.

At the present time, many research groups are reporting on the preparation of PANI/SWCNTs composites by various synthetic techniques. Lie et al. reported SWCNT/PANI composites synthesized by *in situ* electrochemical polymerization processes and investigated their electrochemical properties.[7] Gupta et al. synthesized PANI/SWCNT composites by *in situ* potentiostatic deposition of PANI onto SWCNTs and examined the microstructures and specific capacitances.[8] The same groups also studied the capacitive and energy−power characteristics of PANI/SWCNTs composites prepared by *in situ* electrochemical polymerization techniques.[9] Abdiryim et al. reported the preparation of PANI/SWCNTs composites as electrode materials for supercapacitors by using solid-state synthesis methods.[10] The electrochemical properties of the

Received: October 23, 2013
Revised: February 24, 2014
Published: April 7, 2014

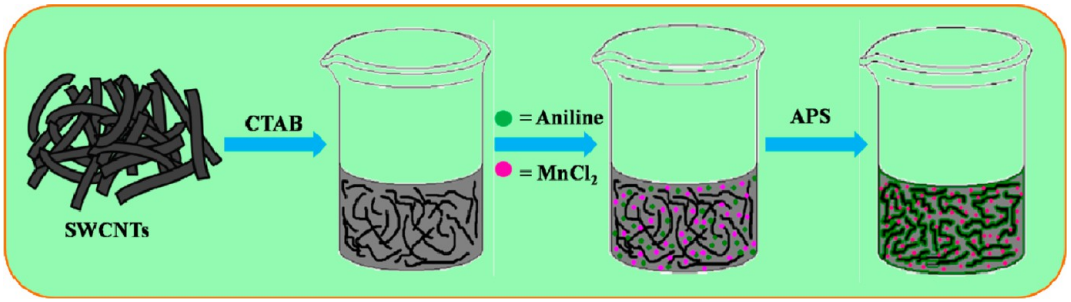

Figure 1. Schematic representation of the nanocomposites synthesis process.

well-coated SWCNTs with PANI composites were investigated by Zhou et al.[11] This group also investigated the supercapacitive properties of SWCNT/PANI composites prepared by *in situ* electrochemical polymerization techniques.[12] Huang et al. studied the electrochemical characteristics of the well-dispersed SWCNT/PANI composite films synthesized by an electrochemical polymerization method.[13] A dye-sensitized solar cell based on PANI/SWCNT composites was studied by Abdel-Fattah et al.[14] Lie et al. synthesized SWCNT/PANI composite films by *in situ* electrochemical polymerization processes and investigates their thermoelectric properties.[15] The charge transport phenomenon of the PANI/SWCNT composites was examined by Granot et al.[16] Ramamurthy et al. reported on the fabrication and electrical characterization of metal−semiconductor devices for PANI/SWCNT composites.[17] The fabrication of amperometric triglyceride biosensor based on electrochemically deposited PANI/SWCNT composite film onto an indium−tin oxide glass plate was investigated by Dhand et al.[18] Yan et al. synthesized SWCNT/PANI composites by *in situ* polymerization techniques and studied the electrochemical properties.[19] Both fuel cells and the supercapacitive properties of the SWCNT/PANI composites were investigated by Mikhaylova et al.[20] Patil et al. reported on the manganese (Mn)-doped and undoped PANI synthesized by a sonochemical method via dip-coating techniques and investigated the electrochemical properties.[21] To the best of our knowledge, there are no research articles available on transition metal-doped PANI/SWCNT nanocomposites for supercapacitor electrodes. So our motivations for this present study are to synthesize manganese chloride ($MnCl_2$)-doped PANI in the presence of SWCNTs and investigate their potential to be used as superior electrode materials for supercapacitor applications. Generally, our goal in this study is to achieve a new electrode material with superior supercapacitive properties.

Herein, we report that $MnCl_2$-doped PANI/SWCNT nanocomposites [Mn-PANI/SWCNT], $MnCl_2$-doped PANI [Mn-PANI], and pure PANI were synthesized via *in situ* oxidative polymerization techniques by using ammonium persulfate (APS) as oxidant in a HCl medium and were investigated as the electrode materials for supercapacitors. The electrochemical characterization of all the electrode materials were carried out by a two-electrode system, where platinum was used as the counter electrode, which also acted as the reference electrode. The supercapacitive properties of all the electrode materials were studied by cyclic voltammetry (CV), galvanostatic charge/discharge (GCD), and electrochemical impedance spectroscopy (EIS) analysis. Additionally, the electrical, morphological, thermal properties, as well as chemical interaction of all the electrode materials, were also studied.

EXPERIMENTAL SECTION

Materials Used. The aniline monomer, ammonium persulfate (APS), and HCl used in this study were supplied by Merck, Germany. Manganese chloride ($MnCl_2$) was obtained from Sigma-Aldrich, India. SWCNT was obtained from US Research Nanomaterials, Inc., U,S,A. These SWCNTs have lengths of 5−30 μm and diameters of 1.5 nm. Cetyltrimethylammonium bromide (CTAB) was purchased from Loba Chemie Pvt. Ltd., Mumbai, India. Dimethylformamide (DMF) was supplied by Merck, Germany.

Doping on Polyaniline. The $MnCl_2$-doped PANI was synthesized via an *in situ* oxidative polymerizations method using APS as oxidant in a 1.5 M HCl medium. In a 1.5 M 70 mL HCl solution, 1 mL of aniline monomer was added and stirred for 10 min. Then, the $MnCl_2$ solution was prepared by dissolving the $MnCl_2$ in deionized water. This $MnCl_2$ solution was added to the as-prepared aniline solution and further stirred for 10 min. After that, 2.04 g of APS was dissolved in a 1.5 M 60 mL HCl solution. This APS solution was then added drop by drop to the $MnCl_2$-doped aniline solution. Then, the whole solution was stirred for 5 h at a constant speed in room temperature. When the polymerization process was over, the whole solution was filtered, washed with deionized water and ethanol several times, and dried at 75 °C for 12 h. The pure PANI was also synthesized by the same procedure without the addition of $MnCl_2$.[22]

Synthesis of Mn-PANI/SWCNT Nanocomposites. A typical *in situ* chemical oxidative polymerization technique was followed for the synthesis of the nanocomposites. In 150 mL 1.5 M HCl solutions, 1.24 g of CTAB and 50 mg of SWCNTs were added and sonicated for 1 h at room temperature. In another beaker, 1 mL of aniline monomer was dissolved in a 1.5 M HCl solution, and into this solution, we have add a $MnCl_2$ solution and stirred for 10 min. This $MnCl_2$-doped aniline solution was then added to the well-dispersed suspension of SWCNTs solution and stirred for another 15 min. Then, APS solution (by dissolving 2.04 g of APS in deionized water) was added to the above solution and stirred for 5 h at a constant speed and at room temperature. Then, the color change from black to greenish black, which indicated the polymerization, was over. After that the total solution was kept at 1−5 °C for 12 h. The entire solution was filtered and then washed with deionized water and ethanol several times, and then vacuum-dried at 75 °C for 12 h to get the $MnCl_2$-doped PANI/SWCNT nanocomposites. The schematic representation of the synthesis of the nanocomposites is depicted in Figure 1. The compositions of all the electrode materials are summarized in Table 1.

CHARACTERIZATION

FTIR Analysis. To understand the possible interaction between Mn^{2+} with the PANI chains, a FTIR analysis was performed.

Table 1. Composition of the composites

sample codes	polyaniline (wt %)	$MnCl_2$ (wt %)	SWCNTs (wt %)
PANI	100	0	0
Mn-PANI	98	2	0
Mn-PANI/SWCNT	93	2	5

dx.doi.org/10.1021/sc5000072 | ACS Sustainable Chem. Eng. 2014, 2, 1114−1127

The FTIR analysis of the electrode materials was carried out by using a NEXUS 870 FT-IR (Thermo Nicolet) instrument in the range from 4000 to 400 cm^{-1}. The samples were prepared by mixing of spectroscopic grade potassium bromide (KBr) and the electrode materials at a weight ratio of 10:1 and then were pelletized to make disks. The disks were analyzed to obtain the spectra.

UV−Visible Spectroscopy. The UV−visible spectra of all the electrode materials were performed by using a PerkinElmer Lambda 750 spectrophotometer. The UV−visible spectra were taken between 200 and 800 nm wavelength regions. All the electrode materials were dissolved in a DMF solvent for UV−visible spectroscopy analysis.

Raman Analysis. Raman spectroscopy was performed in order to check the interfacial bonding between Mn^{2+} with PANI and also Mn^{2+}-doped PANI with SWCNTs. Raman spectra of all of the electrode materials were recorded with a RAMNOR HG-2S spectrometer (Jobin-Yvon, France) by an argon ion laser with 10 mW power.

X-ray Diffraction Study. X-ray diffraction characteristics of all the powder samples were performed by using a PW X-ray diffractometer with a Cu Kα target (λ = 0.15404 nm) at 2 mm slits at a scanning rate of 2° per min with current and operating voltage at 20 mA and 40 kV, respectively. The X-ray diffraction analysis was carried out for all the electrode materials in the 2θ ranges from 10° to 75°.

Field Emission Scanning Electron Microscopy (FESEM) Analysis. A field emission scanning electron microscope (Carl Zeiss-SUPRA 40 FESEM) was used to investigate the surface morphology of PANI, Mn-PANI, and Mn-PANI/SWCNT nanocomposites and also the coating of Mn-doped PANI over the SWCNTs surfaces. The power samples were dispersed in acetone and put dropwise in the aluminum foil and dried at room temperature. This dried foil was then placed into the carbon tap and sputter coated with gold. The FESEM micrographs were taken at an operating voltage of 40 kV. To check the elemental composition of the electrode material, an energy-dispersive X-ray spectroscopy (EDX) analysis was performed.

Transmission Electron Microscopy (TEM) Analysis. To examine the uniformity of the coating of Mn^{2+}-doped PANI on SWCNTs surfaces, high resolution transmission electron microscopy (HR-TEM, JEOL 2100) analyses were carried out. Small amounts of sample were put in the acetone and sonicated for 25 min. From this well-dispersed solution, one drop of solution was put on the copper grid for TEM analysis.

Electrochemical Characterization. All the electrochemical characterization, such as CV, GCC, and EIS analyses, were carried out on a GAMRY Reference 3000 instrument (750 mA and 1.6 V) with a two-electrode system, where platinum was used as the counter electrode, which also acted as the reference electrode. CV measurement was performed in 1 M aqueous KCl solution at different scan rates from 10 to 200 mV/s. The specific capacitances of all the electrode materials were calculated by using the following equation

$$C_s = \frac{\int_{V1}^{V2} i(V)\mathrm{d}V}{(V2 - V1)vm} \quad (1)$$

where the numerator signifies the total charge under the CV curve, $V1$ and $V2$ are the lower and upper voltage limits, v is the scan rate, and m is the mass of the electrode materials. The working electrode was prepared by following procedure. A 1 mg sample was dissolved in 1 mL of 1% nafion solution by sonication for 15 min. That solution was cast onto a glassy carbon electrode having a diameter of 3 mm.[23−26] This electrode was used as the working electrode. The electrode was completely dried before electrochemical characterization. It is reported that the amount of nafion content, in the range of 10−30%, has little influence on specific capacitance, although using of 50% nafion with the carbonaceous supercapacitor electrode showed lower capacitance performances due to its internal resistance. Therefore, we have used a minimum of 1% nafion as binder, which had a very minor effect on cyclic voltammetry measurements.

Electrical Conductivity Measurements. The electrical conductivity of all the electrode materials was calculated by conventional four-electrode methods (Lakeshore resistivity and Hall measurement setup) with compressed pellets. The pellets are prepared by pressing all the electrode materials at 6 MPa pressure. All the pellets were about 0.05 cm thick. The electrical conductivity of all the electrode materials was estimated by using the following equation

$$\rho = \pi t/\ln 2(V/I)$$
$$= 4.53 \times t \times \text{Resistance}$$
$$\text{Conductivity } (\sigma;\ \text{S/cm}) = 1/\rho \quad (2)$$

where ρ is the resistivity in ohms cm, V is the measured voltage, I is the source current, and t is the thickness of the pellets.

Current (*I*)−Voltage (*V*) Relationship. The current−voltage (I−V) feature of the Mn-PANI/SWCNT nanocomposites along with pure PANI and Mn-PANI were recorded by a Keithley 2400 source meter at room temperature and at a 0.1 V/s scan rate.

Thermogravimertic Analysis. To check the thermal stability of the Mn-PANI/SWCNT nanocomposites along with pure PANI and Mn-PANI, thermogravimertic analyses were carried out. The thermal stability of all the electrode materials were analyzed by a thermogravimertic analyzer (TGA 209F, NETZSCH, Germany). The TGA analyses were done with a heating rate of 10 °C/mins under a nitrogen atmosphere.

RESULTS AND DISCUSSION

FTIR Analysis. The structural information on all the electrode materials was identified by FTIR spectra. Figure 2

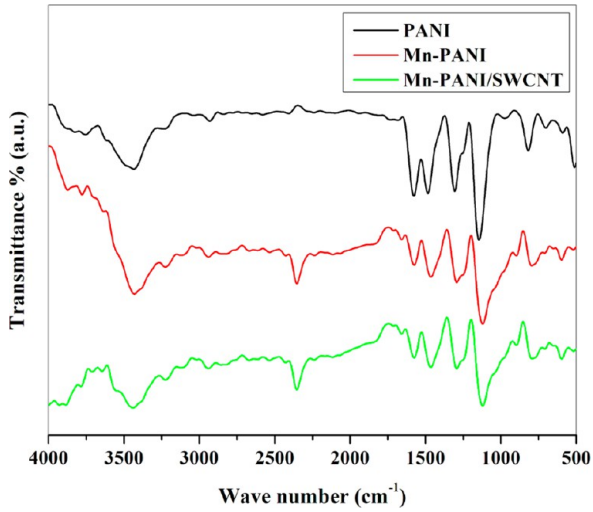

Figure 2. FTIR spectrum of pure PANI, Mn-PANI, and Mn-PANI/SWCNT nanocomposites.

shows the typical FTIR spectra of pure PANI, Mn-PANI, and Mn-PANI/SWCNT nanocomposites. Pure PANI shows all the characteristic bands of the polymer at 1577 cm^{-1} (assigned as C═C stretching of the quinonoid rings), 1481 cm^{-1} (C═C stretching of benzenoid ring), 1305 cm^{-1} (assigned for C−N stretching vibration), 1144 cm^{-1} (ring stretching, N═Q═N, Q signifying the quinonoid ring), and 816 cm^{-1} (C−H out of plane bending vibration).[27,28] All these characteristic bands are present in both Mn-PANI and Mn-PANI/SWCNT nanocomposites with some shifting of peaks. The peaks at 1577 cm^{-1} shifted to 1573 and 1574 cm^{-1} for Mn-PANI and Mn-PANI/SWCNT nanocomposites, respectively, and the peaks at 1481 cm^{-1} shifted to 1463 and 1465 cm^{-1} for Mn-PANI and Mn-PANI/SWCNT nanocomposites, respectively. The peaks at 1305 cm^{-1} shifted to 1291 and 1293 cm^{-1} for Mn-PANI and Mn-PANI/SWCNT nanocomposites, respectively. It is also observed that the bands at 1144 cm^{-1} shifted to

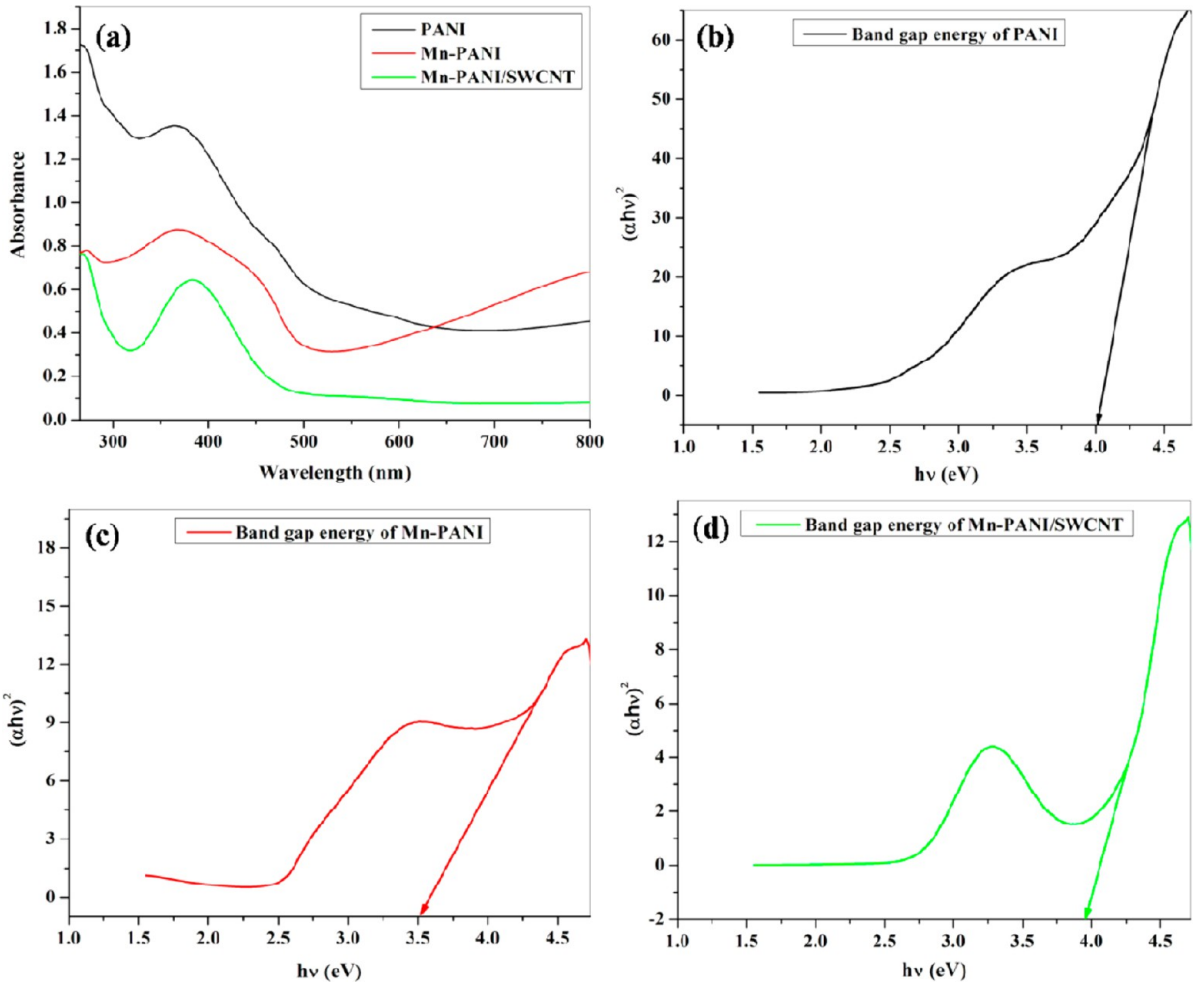

Figure 3. UV−visible spectra of (a) PANI, Mn-PANI, and Mn-PANI/SWCNT nanocomposites, and band gap energy of (b) PANI, (c) Mn-PANI, and (d) Mn-PANI/SWCNT nanocomposites.

1119 and 1120 cm^{-1} for Mn-PANI and Mn-PANI/SWCNT nanocomposites, respectively, and the bands at 816 cm^{-1} shifted to 795 and 786 cm^{-1} for Mn-PANI and Mn-PANI/SWCNT nanocomposites, respectively. This interesting phenomenon specifies there is a good interaction between Mn and PANI and also confirmed the doping of Mn in the PANI.[21] For Mn-PANI/SWCNT nanocomposites, the shifting of peaks at lower wavelength is mainly due to the $\pi-\pi$ conjugated interaction between the benzene ring of PANI and the graphite-structured SWCNTs, indicating a strong interaction between SWCNTs and the PANI.[29,30] For all the electrode materials, a broad band is observed at around 3420 cm^{-1}, and the characteristic peaks at 3221 cm^{-1} were because of the N−H stretching vibration. Further, the absorption bands at 2930 and 2850 cm^{-1} correspond to C−H stretching vibrations.

UV−Visible Spectroscopy Analysis. To check the electronic properties of the PANI and the nanocomposites, UV−visible absorption spectroscopy analyses were performed. Figure 3(a) represents the UV−visible spectra of the pure PANI, Mn-PANI, and Mn-PANI/SWCNT nanocomposites. Pure PANI shows three characteristic absorption peaks at 368, 466, and 592 nm. The absorption peak at 368 nm is assigned to the $\pi - \pi^*$ transition of the benzene rings. The peak at 466 nm is for the polaron−π^* transition, and the absorption peak at 592 nm is attributed to electronic transitions in the EB from of PANI.[31,32] The absorption peak at 368 nm shifted to higher wavelengths at 373 and 384 nm for the Mn-PANI and Mn-PANI/SWCNT nanocomposites, respectively. This red-shifting phenomenon of the absorption peak in Mn-PANI may be due to the doping effect. It is also observed that there is a red shifting of the peak for the Mn-PANI/SWCNT nanocomposites, only because of some interaction between the the quinonoid ring of PANI and SWCNTs.

For semiconductors, the band gap is the energy gap between the valence band and the conduction band. But for conducting polymers, the band gap is defined as the least photon energy required for exciting an electron from the highest occupied molecular orbital (HOMO) to the lowest unoccupied molecular orbital (LUMO). In both the cases, the band gap is decreased by the incorporation of doping agents inside the materials. The band gap was calculated by means of the Tauc equation[33]

$$\alpha h\nu = B(h\nu - E_g)^n \tag{3}$$

where α is the absorption coefficient, h is the Planck constant, ν represents the photon frequency, B is a fitting parameter, E_g is the band gap, and n is the different possible electronic transitions responsible for the light absorption. For PANI and its derivatives, $n = 1/2$.[34] The band gap was obtained by plotting the UV−visible spectra as $(\alpha h\nu)^2$ vs $h\nu$ and extrapolating the linear portion of $(\alpha h\nu)^2$ vs $h\nu$ to zero, shown in Figure 3(b−d). The calculated E_g values were 4, 3.51, and

dx.doi.org/10.1021/sc5000072 | ACS Sustainable Chem. Eng. 2014, 2, 1114−1127

3.95 eV for the pure PANI, Mn-PANI, and Mn-PANI/SWCNT nanocomposites, respectively. The blue shift of the band gap for the Mn-PANI and Mn-PANI/SWCNT nanocomposites clearly indicates that the metal ions strongly bind with the PANI chain as well as the SWCNTs.

Raman Analysis. Figure 4 shows the Raman spectra of the pure PANI, Mn-PANI, and Mn-PANI/SWCNT nanocomposites.

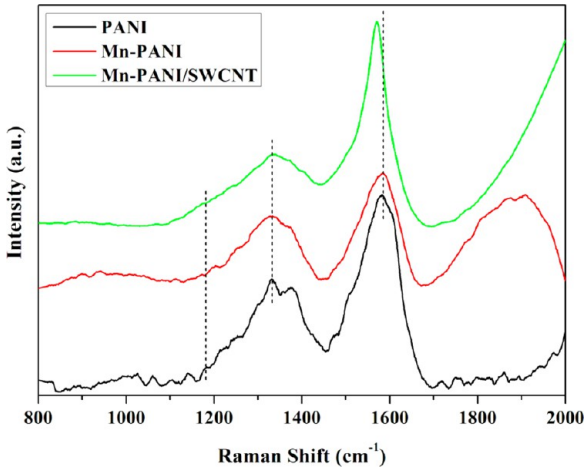

Figure 4. Raman spectra of pure PANI, Mn-PANI, and Mn-PANI/SWCNT nanocomposites.

The Raman spectrum of pure PANI show bands at 1181 cm^{-1} for C−H bending of the quinonoid/benzenoid ring, 1332 cm^{-1} for C−$N^{+\bullet}$ stretching of the bipolaron structure, and 1583 cm^{-1} mainly due to the C−C stretching of the benzenoid ring.[35] These bands confirm the chemical structure of PANI. The same type of spectrum is also observed for Mn-doped PANI, and it is noticed that the intensity decreases compared to PANI. The decrease in intensity is mainly due to the doping effect.[21] The characteristic band at 1332 cm^{-1} shifted to a lower wave at 1328 cm^{-1}, and also the decrease in intensity indicated the presence of Mn in PANI.[21] The band at 1583 cm^{-1} shifted to a lower wavelength at 1570 cm^{-1}, which is close to the G band of the SWCNTs and is observed for the Mn-PANI/SWCNT nanocomposites. Here, the peak becomes sharper compared to PANI and also shifted to a lower wavelength mainly because of the $\pi-\pi^*$ electron interaction between the PANI and the SWCNTs.[36]

XRD Analysis. Figure 5 represents the XRD pattern of the pure PANI, Mn-PANI, and Mn-PANI/SWCNT nanocomposites. For pure PANI, three crystalline peaks appear at 2θ = 15.13°, 20.10°, and 25.36°, corresponding to (011), (020), and (200) crystalline planes of PANI in its emeraldine salt form, respectively.[37] For Mn-PANI, one additional broad peak is observed at 2θ = 29−31°. This broad peak in the XRD pattern indicates the presence of $MnCl_2$ within in the Mn-PANI composite.[38] With the incorporation of the SWCNTs into the doped PANI matrix, the sharp and strong diffraction peak at 2θ = 25.36° is observed for SWCNTs,[39] which overlaps with the peak of PANI that results in the intense and broad peak of the Mn-PANI/SWCNT nanocomposites.

Surface Morphology Study. The surface morphology of the as-prepared Mn-PANI/SWCNT nanocomposites along with pure PANI and Mn-PANI was investigated by FESEM analysis. Figure 6 shows the typical FESEM images of pure PANI, Mn-doped PANI, pristine SWCNTs, and Mn-PANI/SWCNT

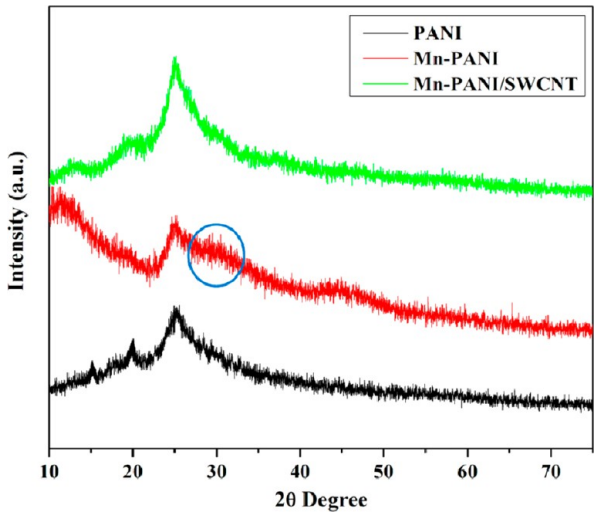

Figure 5. XRD patterns of pure PANI, Mn-PANI, and Mn-PANI/SWCNT nanocomposites.

nanocomposites, respectively. The granular with agglomerated structure is observed for PANI, shown in Figure 6(a). The granular-like morphology is more distinct for Mn-PANI composites, shown in Figure 6(b). The little difference in morphology of Mn-PANI compared to pure PANI is mainly due to the doping effect. Here, the transition metal ion (Mn^{2+}) has several positions for doping and tends to bind different nitrogen sites of PANI, and by coordination, they form interchain linkage among various adjacent PANI chains. Figure 6(c) depicts the FESEM images of pristine SWCNTs. It is clearly shown that the SWCNTs bundles are randomly oriented together to form a three-dimensional (3D) network structure. Here, the average diameter of the SWCNTs is 1−5 nm. The FESEM images of the Mn-PANI/SWCNT nanocomposites is shown in Figure 6(d), and it is observed that the SWCNTs surface is uniformly coated by Mn-doped PANI. Here, the average diameter of the SWCNTs is 10−15 nm. This increase in the diameter of SWCNTs is due to the coating.

To check the presence of $MnCl_2$ in the Mn-PANI/SWCNT nanocomposites, energy-dispersive X-ray (EDX) spectroscopy analysis was done. The typical EDX spectrum of a Mn-PANI/SWCNT nanocomposites is shown in Figure 7. From the EDX spectrum, it is confirmed that the both Mn and Cl are present in the Mn-PANI/SWCNT nanocomposites.

TEM Analysis. The typical TEM micrographs for the pure PANI, Mn-PANI, and Mn-PANI/SWCNT nanocomposites are shown in Figure 8. Figure 8(a) represents the TEM image of pristine PANI. It is shown from Figure 8(b) that there is a presence of a black spherical portion in the PANI surface (red circles). The black portion appearing in the TEM image is due to Mn^{2+}, which is from $MnCl_2$. Figure 8(c) depicts the TEM image of pure SWCNTs. It is observed that these SWCNTs are curved and have a coil-like structure with diameters of 1−5 nm. The uniform coating of Mn-doped PANI over the SWCNTs surface with the presence of black spherical Mn^{2+} (red circles) is observed, shown in Figure 8(d). Here, the average diameter of the coated SWCNTs was 15−20 nm. The increase in the diameter is due to the coating by Mn-doped PANI. A possible explanation for the appearance of the black spherical portion in the TEM images can be explained by the coordination principle. Here, the Mn^{2+} ion may bind with the nitrogen atoms of PANI chains. So, Mn^{2+} can form interchain linkage among

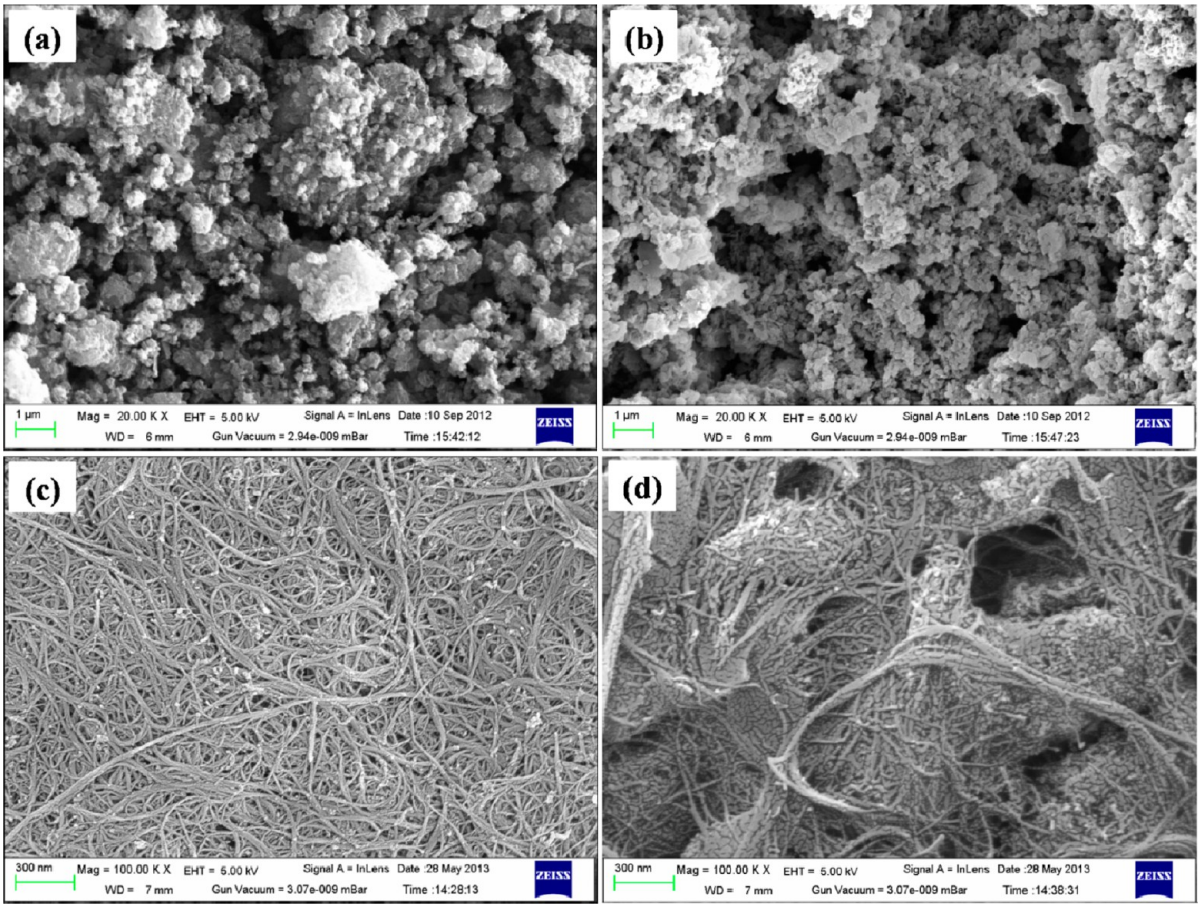

Figure 6. FESEM micrographs of (a) pure PANI, (b) Mn-PANI, (c) pristine SWCNTs, and (d) Mn-PANI/SWCNT nanocomposites.

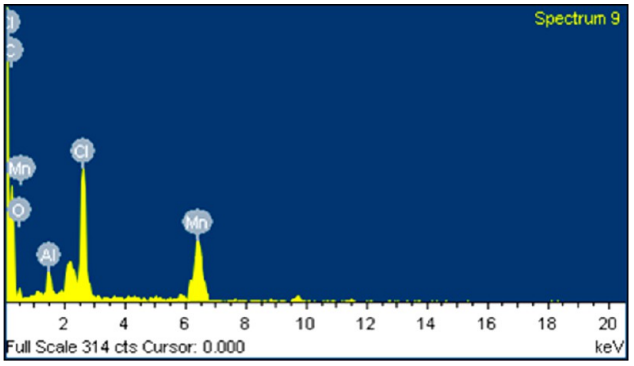

Figure 7. EDX spectra of Mn-PANI/SWCNT nanocomposites.

several adjacent PANI chains by coordination both by intrachain and interchain connections, which led to the more black spherical conformation or aggregation in the Mn-PANI and Mn-PANI/SWCNT nanocomposites.[40] After addition of the aniline monomer into the SWCNTs solutions, the interaction corresponded to the $\pi-\pi^*$ electron interaction between the SWCNTs, and the aniline monomer is the main reason behind the uniform coating over the SWCNTs surface.[41]

Electrochemical Characterization. Electrochemical characterizations of the as-prepared Mn-PANI/SWCNT nanocomposites along with pure PANI and Mn-PANI were investigated by cyclic voltammetry (CV), galvanostatic charge/discharge (GCD), and electrochemical impedance spectroscopy (EIS) analysis. A 1 M aqueous KCl solution was used as the electrolyte for all the electrochemical characterizations.

Cyclic Voltammetry. CV gives the information about the reversible nature of the electrode in an appropriate electrolyte and also the effect of scan rate on specific capacitance. Figure 9(a–c) presents the CV curves of pure PANI, Mn-PANI, and Mn-PANI/SWCNT electrodes within the potential window from −0.8 to 0.8 V. The CV curves of all the electrode materials were taken at different scan rates of 10, 20, 50, 100, and 200 mV/s in a 1 M KCl solution. From the CV curve of all of the electrode materials, it is observed that the redox peaks are absent, although the redox active materials are present that signifies that charging/discharging takes place at a pseudo-constant rate over the entire voltammetric cycles. The rectangular shape of the CV curves shows the ideal pseudocapacitive nature of the electrode. By using eq 1, we have calculated the specific capacitance of all the electrode materials, and their values at different scan rates are given in Table 2.

It is observed that the Mn-PANI/SWCNT nanocomposites show the highest specific capacitance of 548 F/g at a 10 mV/s scan rate, whereas pure PANI and Mn-PANI exhibit specific capacitance of 395 and 475 F/g at a 10 mV/s scan rate, respectively. The higher specific capacitance value of Mn-PANI compares to pure PANI mainly because of transition metal doping.[42] The maximum specific capacitance of the Mn-PANI/SWCNT nanocomposites may be due to these possible reasons: (i) The presence of a highly accessible surface area of the SWCNTs in the Mn-PANI/SWCNT nanocomposites improves the specific capacitance. (ii) With transition metal ion

dx.doi.org/10.1021/sc5000072 | ACS Sustainable Chem. Eng. 2014, 2, 1114−1127

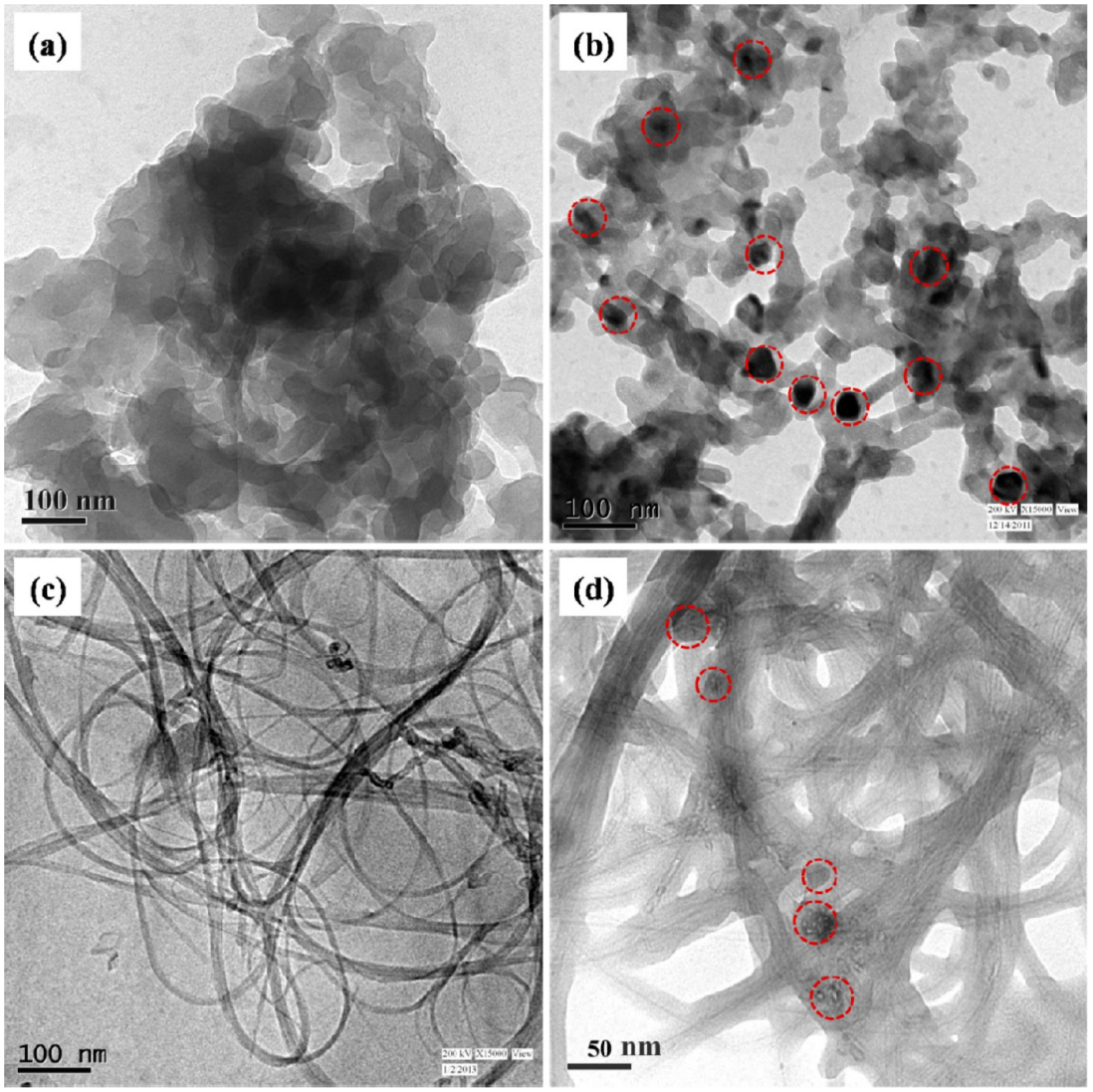

Figure 8. TEM micrographs of (a) pure PANI, (b) Mn-PANI, (c) pristine SWCNTs, and (d) Mn-PANI/SWCNT nanocomposites.

(Mn^{2+}) doping, Mn^{2+} co-ordination with a lone pair or one-electron donation from the N atom of PANI enhances the capacitance. (iii) The uniform coating of $MnCl_2$-doped PANI over SWCNTs surfaces enhances capacitance. (iv) In the early stage of oxidative polymerization techniques, there is a strong interaction between the π-bonded SWCNTs surface with the conjugated structure of the PANI, which helps the deposition of polymer chains over the SWCNTs surface. With the strong $\pi-\pi$ interaction among PANI and SWCNT, there is a possibility of charge transfer from planar polymer chains to SWCNTs, which increases the active sites for faradic reactions and thereby enhances the specific capacitance.[43] For Mn-PANI/SWCNT nanocomposites, the Mn^{2+} ion is coordinated with PANI simultaneously with the SWCNTs surface, and greater accumulation of charge occurs. Therefore, greater specific capacitance was observed compared to pure PANI and Mn-PANI electrode materials. The specific capacitance value in our study is quite high compared to some of the reported articles on PANI/SWCNT or Mn-doped PANI composites. A comparison of the specific capacitance obtained for Mn-PANI/SWCNT nanocomposites with the data reported for PANI/SWCNT or Mn-doped PANI electrodes are summarized in Table 3.

The plot of specific capacitance vs scan rate is shown in Figure 10. It is observed that with an increase in the scan rate the specific capacitance of all the electrode materials decreases. The decrease in the specific capacitance at higher scan rates is due to the diffusion effect of proton within the electrode, while at low scan rates it is due to the occurrence of inner active sites, which undergo complete redox transitions and enhance the specific capacitance.[44]

Galvanostatic Charge/Discharge. To estimate the electrochemical performance of the electrode materials under constant current conditions, galvanostatic charge/discharge is the faithful method. The galvanostatic charge/discharge plot of pure PANI, Mn-PANI, and Mn-PANI/SWCNT nanocomposites at a constant current density of 0.5 A/g is depicted in Figure 11(a). The charge/discharge experiment for all the electrode materials was done within the potential window from −0.8 to 0.8 V. The constant current charge/discharge plot of PANI shows two stages of voltage drops from 0.8 to 0.75 V and 0.75 to −0.8 V. The charge/discharge plots of Mn-PANI and Mn-PANI/SWCNT shows some extant similar in nature with the two stages of voltage drops, 0.8 to 0.78 and 0.78 to −0.8 V for Mn-PANI and 0.8 to 0.70 and 0.70 to −0.8 V for Mn-PANI/SWCNT nanocomposites. It is observed that there is a fast

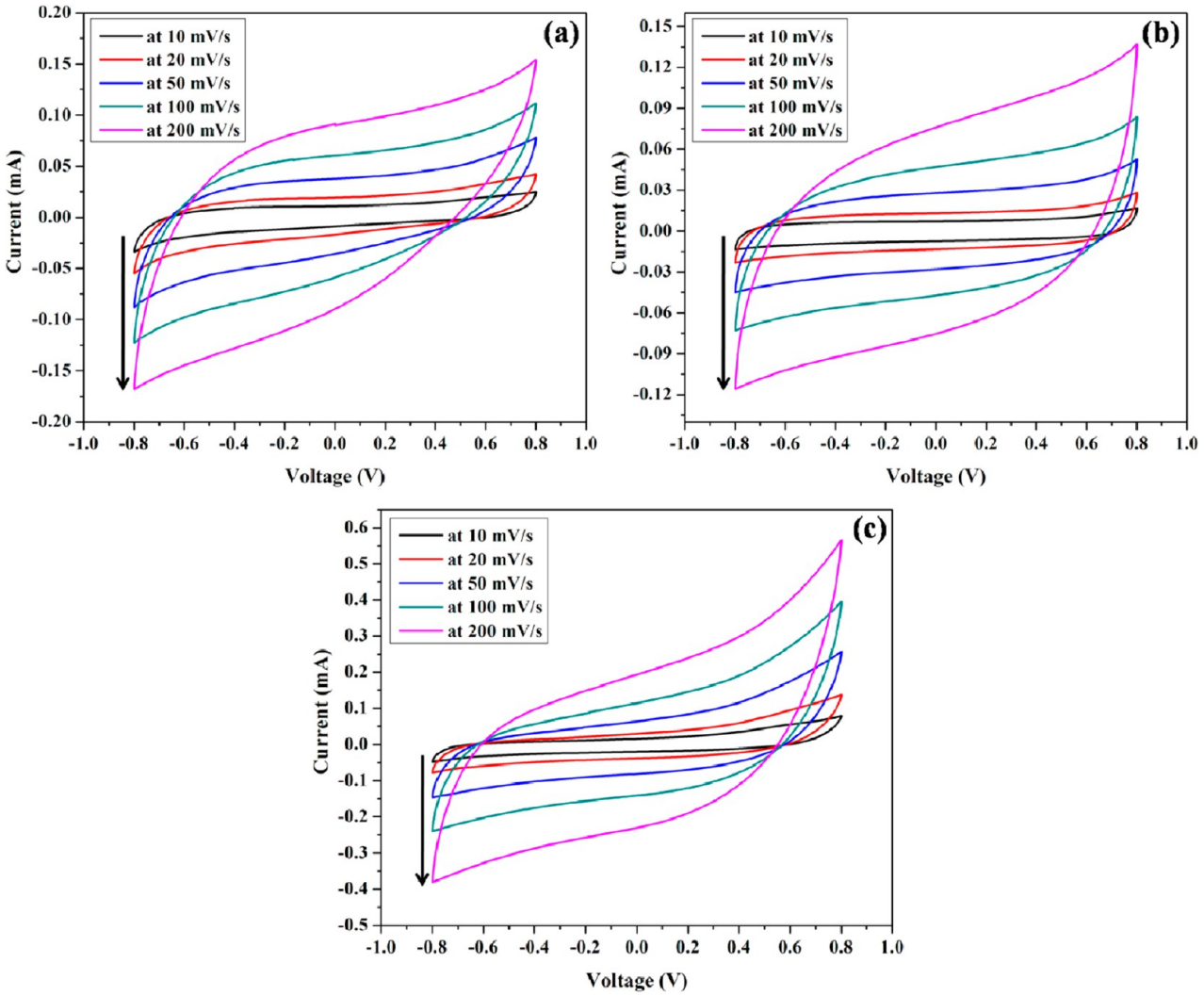

Figure 9. Cyclic voltammogram at different scan rates of (a) pure PANI, (b) Mn-PANI, and (c) Mn-PANI/SWCNT nanocomposites.

Table 2. Specific Capacitance of PANI, Mn-PANI, and Mn-PANI/SWCNT Nanocomposites at Different Scan Rates

sample	10 mV/s	20 mV/s	50 mV/s	100 mV/s	200 mV/s
PANI	395	341	258	198	142
Mn-PANI	475	414	335	270	211
Mn-PANI/SWCNT	548	487	392	327	257

Table 3. Comparison of Specific Capacitance of PANI/SWCNT and Mn-PANI Supercapacitor Electrodes with Literature Data

electrode materials	measurement type	electrolyte	working electrode	specific capacitance (F/g)	references
PANI/SWCNTs	3-electrode	1 M $NaNO_3$	Ni-foam current collector (1 cm × 1 cm)	190.6	11
PANI/SWCNTs	3-electrode	1 M H_2SO_4	stainless steel sheet (1 cm × 1 cm)	485	9
PANI/SWCNTs	3-electrode	1 M $HClO_4$ + 3 M $NaClO_4$	Ni-foam current collector (1 cm × 1 cm)	311.7	12
PANI/SWNTs	3-electrode	1 M H_2SO_4	Ni wire	501.8	7
PANI/SWCNTs	3-electrode	1 M H_2SO_4	stainless steel sheet (1 cm × 1 cm)	463	8
PANI/SWCNTs	3-electrode	1 M H_2SO_4	graphite current collector	423	10
PANI/SWCNTs	3-electrode	0.5 M H_2SO_4	glassy carbon electrode	400	20
Mn/PANI	3-electrode	1 M H_2SO_4	–	474	21
Mn-PANI/SWCNT	2-electrode	1 M KCl	glassy carbon electrode	548	present work

discharge within the first potential region, whereas relative delay in the second potential region, indicating superior specific capacitance. For Mn-PANI/SWCNT nanocomposites, the short discharge duration (in the range from 0.8 to 0.70 V) is attributed to the EDLC, whereas the longer discharge duration (in the range from 0.70 to −0.8 V) is ascribed to the combination of both EDLC and the pseudocapacitance. The IR drops designated the internal resistance of the electrode

dx.doi.org/10.1021/sc5000072 | ACS Sustainable Chem. Eng. 2014, 2, 1114−1127

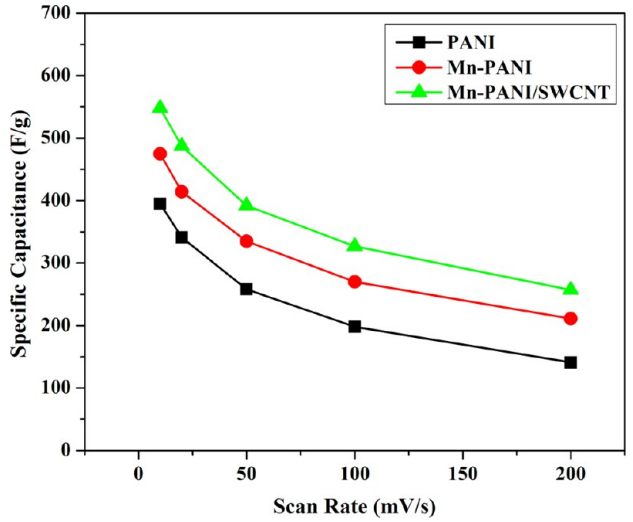

Figure 10. Plot of specific capacitance vs scan rate.

material, which increases with an increase in current density. Low internal resistance is a significant factor in energy-storing devices because less energy will be wasted to generate unwanted heat in charging/discharging processes. The galvanostatic charge/discharge plots of all the electrode materials at different current densities of 0.5, 1, 1.5, 2, and 3 A/g are shown in Figure 11(b–d). It is observed that for all the electrode materials the discharge time decreases with an increase in the current density.

The specific capacitance value of all of the electrode materials was again determined from charge/discharge profiles by using the following equation

$$\text{Specific Capacitance, } C_s = \frac{i \times t}{\Delta\nu \times m} \tag{4}$$

where i and m represent the current density in A/g, $\Delta\nu$ is the potential range, and t represents the discharge time in seconds. The highest specific capacitance of 546 F/g was obtained for Mn-PANI/SWCNT nanocomposites at 0.5 A/g current density. For PANI and Mn-PANI, the specific capacitances of 389 and 476 F/g were obtained at the same current density. It is observed for all of the electrode materials that with an increase in current density the specific capacitance value slowly decreases. By using eq 4, the specific capacitance values at different current densities were calculated and are shown in Table 4.

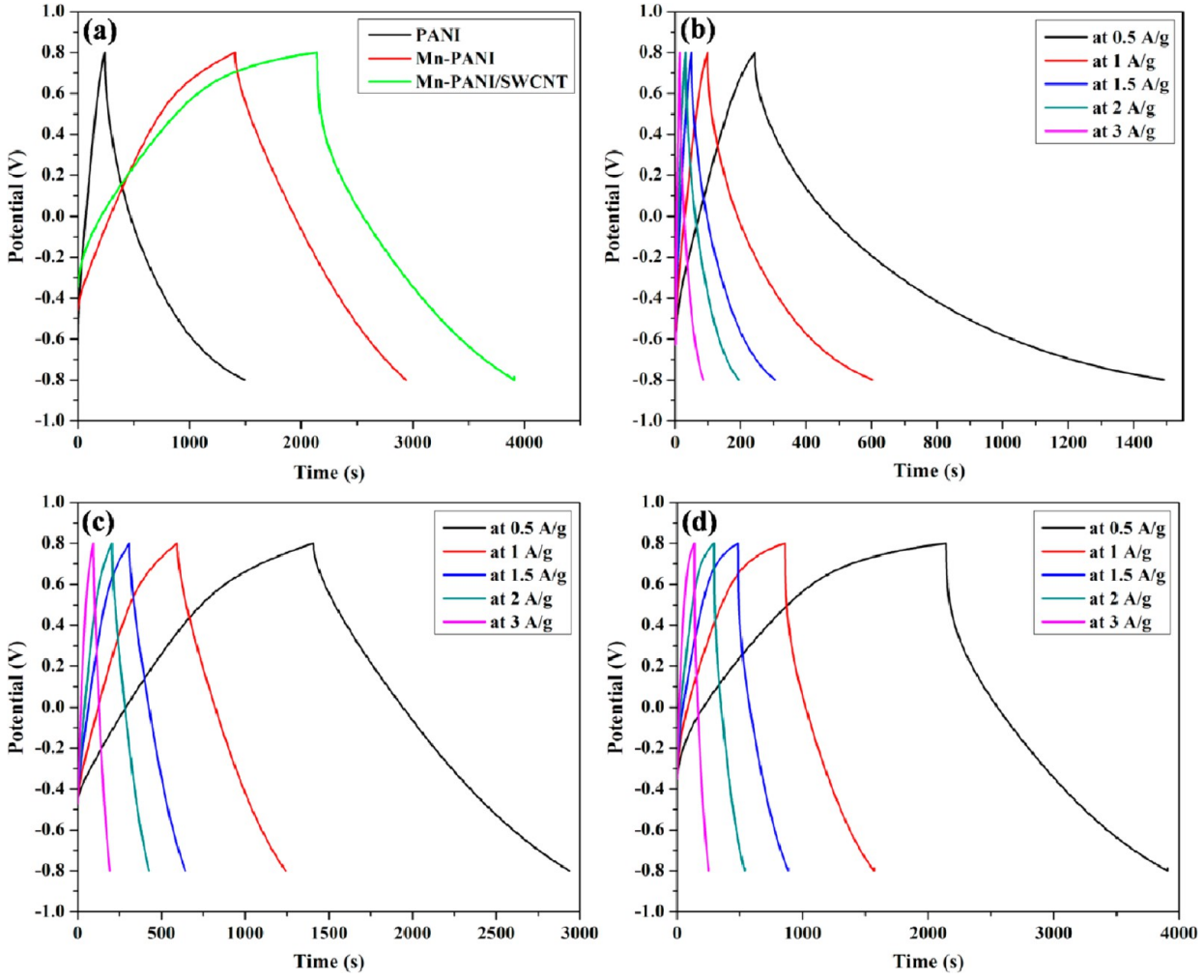

Figure 11. Comparative galvanostatic charge/discharge plot of pure PANI, Mn-PANI, and Mn-PANI/SWCNT nanocomposites at a constant charge/discharge current density of 0.5 A/g. GCD plots at different current density of 0.5, 1, 1.5, 2, and 3 A/g for (b) pure PANI, (c) Mn-PANI, and (d) Mn-PANI/SWCNT nanocomposites.

dx.doi.org/10.1021/sc5000072 | ACS Sustainable Chem. Eng. 2014, 2, 1114–1127

Table 4. Specific Capacitance of PANI, Mn-PANI, and Mn-PANI/SWCNT Nanocomposites Obtained from Galvanostatic Charge/Discharge Profiles at Different Current Densities

sample	0.5 A/g	1 A/g	1.5 A/g	2 A/g	3 A/g
PANI	389	315	237	201	135
Mn-PANI	476	407	314	277	187
Mn-PANI/SWCNT	546	444	378	302	221

The supercapacitive properties of a material also depend on energy density as well as power density. The main disadvantage of the supercapacitors electrode materials is low energy density. In this study, all the electrode materials showed better energy density as well as power density. The energy density and power density values were obtained from charge/discharge profiles. The energy density of all the electrode materials was calculated by using following equation

$$\text{Energy Density } (E) = 1/2(CV^2) \quad (5)$$

where C is the specific capacitance obtained from the GCD profile, and V is the operating voltage. The power density of all the electrode materials was obtained by using the following equation

$$\text{Power Density } (P) = E/t \quad (6)$$

where t is the discharge time obtained from GCD profile.

The energy densities of pure PANI, Mn-PANI, and Mn-PANI/SWCNT nanocomposites at different current densities are shown in Table 5. The highest energy density of 194.13 Wh/kg is obtained for Mn-PANI/SWCNT nanocomposites at 0.5 A/g current density. The power densities of all the electrode materials at various current densities are given in Table 6. The maximum power density of 2571.38 W/kg is obtained for Mn-PANI/SWCNT nanocomposites at 3 A/g current density. The plot of energy density vs power density (Ragon plot) is given in Figure 12. From the Ragon plot, it is observed that the Mn-PANI/SWCNT nanocomposites exhibit the highest energy density as well as maximum power density compared to pure PANI and Mn-PANI. Here, both the transition metal and SWCNTs play a vital role for enhancement of the electrochemical behavior. It is also noticed that an increase in energy density of the electrode materials occurs with a decrease in power density.

Table 5. Energy Density of PANI, Mn-PANI, and Mn-PANI/SWCNT Nanocomposites at Different Current Densities

sample	0.5 A/g	1 A/g	1.5 A/g	2 A/g	3 A/g
PANI	138.31	112	84.26	71.46	48
Mn-PANI	169.24	142.93	111.64	98.48	66.48
Mn-PANI/SWCNT	194.13	157.86	134.4	107.37	78.57

The cyclic life of the supercapacitor electrode materials is one of the major components for practical applications. The cyclic stability experiment of all the electrode materials was carried out in a 1 M KCl solution. The plot of specific capacitance vs number of cycle at 1 A/g current density is shown in Figure 13.

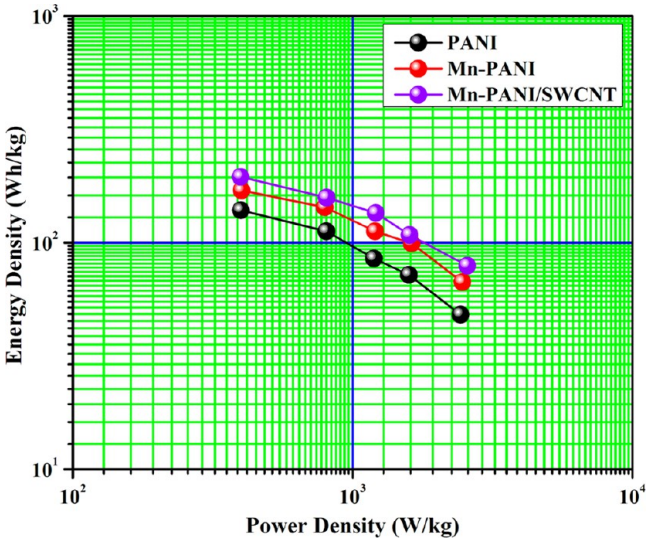

Figure 12. Ragon plot of pure PANI, Mn-PANI, and Mn-PANI/SWCNT nanocomposites.

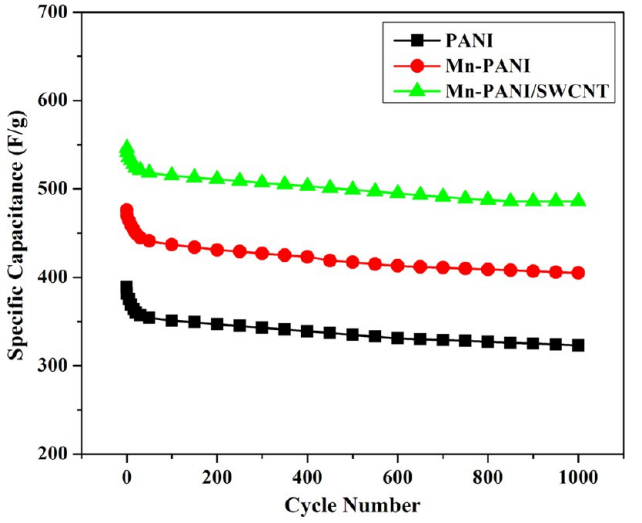

Figure 13. Plot of variation of specific capacitance as a function of cycle number of pure PANI, Mn-PANI, Mn-PANI/SWCNT nanocomposites.

It is observed that the Mn-PANI/SWCNT nanocomposites retain about 88.13% of their original capacitance after 1000 cycles, specifying long-term electrochemical stability. It is also be found that the pure PANI and Mn-PANI exhibited 82.54% and 84.72% specific capacitance retentions after 1000 cycles, respectively. The better cyclic stability of Mn-PANI/SWCNT nanocomposites due to uniform coating of Mn-doped PANI

Table 6. Power Density of PANI, Mn-PANI, and Mn-PANI/SWCNT Nanocomposites at Different Current Densities

sample	0.5 A/g	1 A/g	1.5 A/g	2 A/g	3 A/g
PANI	399	806.4	1189.55	1588	2433.80
Mn-PANI	400.83	795.28	1203.30	1626.27	2467.29
Mn-PANI/SWCNT	397.30	806.09	1209.6	1597.23	2571.38

dx.doi.org/10.1021/sc5000072 | ACS Sustainable Chem. Eng. 2014, 2, 1114−1127

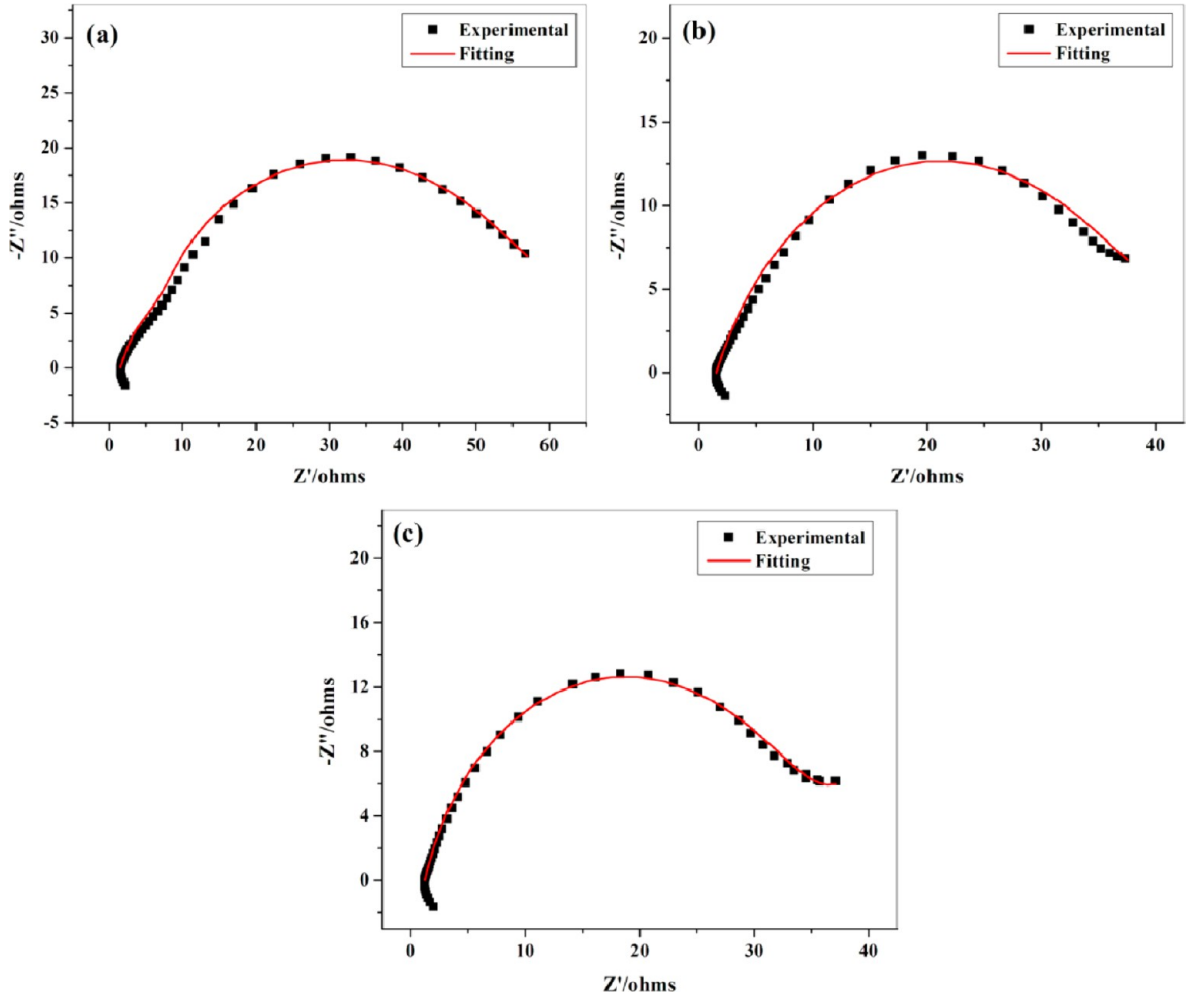

Figure 14. Nyquist plots of (a) pure PANI, (b) Mn-PANI, and (c) Mn-PANI/SWCNT nanocomposites after fitting with an equivalent electrical circuit.

over SWCNTs surfaces increases the active sites of the pseudocapacitance and therefore improves cyclic stability.

Electrochemical Impedance Spectroscopy. To investigate the fundamental behavior of the electrode materials for supercapacitors, EIS analysis was carried out. By using Nyquist plots, the EIS data were analyzed, which demonstrate the frequency response of the electrode/electrolyte system and are generally plotted against the imaginary component $(-Z'')$ of the impedance vs the real component (Z') of the impedance. The Nyquist plots are generally interpreted by fitting the experimental data by an equivalent electrical circuit. Figure 14 shows the fitted Nyquist plots of pure PANI, Mn-PANI, and Mn-PANI/SWCNT nanocomposites. The first intercepts of the semicircle on the real axis denotes the value of both ohmic resistance of the electrolyte and the internal resistance of the electrode materials and is represented as solution resistance (R_s). The impedance semicircle in the high frequency region can be represented by an interfacial charge transfer resistance (R_{ct}), and the straight line having a slope of 45° in the medium frequency signifies the Wargburg resistance (W_d). The appropriate equivalent circuit for all the electrode materials is shown in Figure 15, and their fitting data are summarized in Table 7. The solution resistance of 1.52, 1.50, and 1.21 Ω were obtained for pure PANI, Mn-PANI, and Mn-PANI/SWCNT nanocomposites, respectively. The lowest R_s value is obtained for Mn-PANI/SWCNT nanocomposites and specifies the

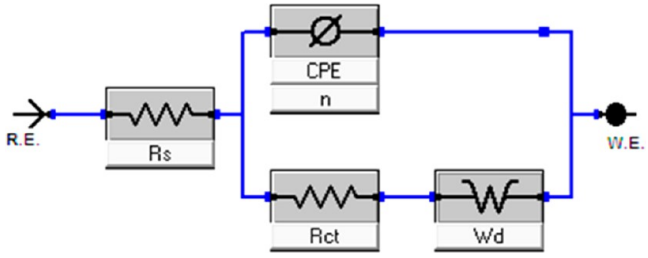

Figure 15. Equivalent circuit used for fitting the Nyquist plots.

superior conductivity as well as specific capacitance. The nanocomposite also achieved the lowest R_{ct} and W_d value. The lowest value for W_d signifys a short diffusive path of the electrolyte ions within the nanocomposites. The main point for a supercapacitor is the frequency factor (n), which can tell us the ideality of a composite toward supercapacitive behavior. The values of n vary between 0 and 1: $n = 0$ specifies the resistor; $n = 1$ indicates the ideal capacitor, which is not possible; and $n = 0.5 - 1$ indicates moderate supercapacitive behavior. All of our synthesized electrode materials showed moderate supercapacitor behavior. The nanocomposites achieved the highest n value of 0.81.

Electrical Conductivity Measurement. The electrical conductivity measurements of the as-prepared electrode

dx.doi.org/10.1021/sc5000072 | ACS Sustainable Chem. Eng. 2014, 2, 1114−1127

Table 7. Fitting Data of Equivalent Circuit Elements Obtained by Simulation of Impedance Spectra

sample	R_s (Ω)	R_{ct} (Ω)	W $(S - s^{0.5}) \times 10^{-2}$	CPE $(S - s^n) \times 10^{-3}$	n
PANI	1.52	59.62	12.9	0.79	0.71
Mn-PANI	1.50	38.08	16.3	1.10	0.74
Mn-PANI/SWCNT	1.21	33.46	7.4	0.43	0.81

Table 8. Electrical Conductivity Measurements

sample	thickness (d, cm)	resistance (ohms)	resistivity (ρ, ohm cm)	conductivity (σ, S/cm)
PANI	0.05	10.72	2.43	0.41
Mn-PANI	0.05	1.35	0.30	3.26
Mn-PANI/SWCNT	0.05	0.45	0.10	9.65

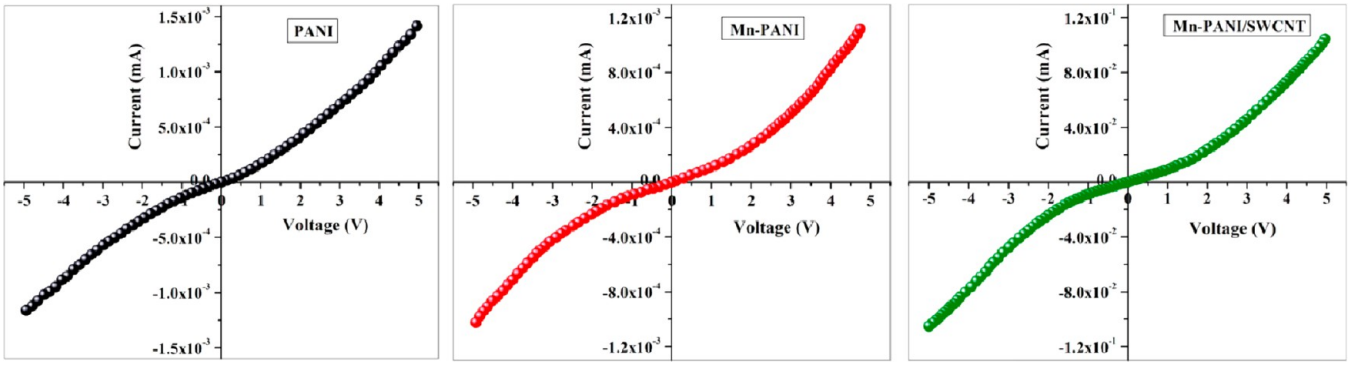

Figure 16. $I-V$ plots of pure PANI, Mn-PANI, and Mn-PANI/SWCNT nanocomposites.

materials were carried out by using four-point probe methods at room temperature, and their values were calculated by using eq 2 and are given in Table 8. It is observed that the pure PANI achieved electrical conductivity of 0.41 S/cm, whereas Mn-PANI showed conductivity of 3.26 S/cm. The increase in the conductivity of Mn-PANI compared to PANI may be due to the doping effect. The highest electrical conductivity of 9.64 S/cm is obtained for Mn-PANI/SWCNT nanocomposites, which is much higher than both PANI and Mn-PANI. This improvement of conductivity may be because of the dopant effect or charge transfer from PANI and the SWCNTs. Additionally, due to the large surface area and high aspect ratio of SWCNTs, which serve as conductive bridges and connecting PANI conducting domains, the electrical conductivity of the nanocomposite is enhanced.[45]

Current (I)−Voltage (V) Characteristics. $I-V$ characteristics of all the electrode materials were measured at room temperature. That experiment was carried out within the potential range from −5 to 5 V, and the $I-V$ curves are shown in Figure 16. For all the electrode materials, the current increases with an increase in the applied voltage in a nonlinear fashion. So, all the electrode materials showed a nonohmic behavior because V/I is not constant. The nonlinearity in the $I-V$ curves signifies the semiconducting behavior. So, all the electrode materials have the capability of making various types of electronic devices.

Thermogravimertic Analysis. The thermal stability of the as-prepared electrode materials was performed by thermogravimertic analysis, and the TGA thermograms of PANI, Mn-PANI, and Mn-PANI/SWCNT nanocomposites are shown in Figure 17. For both PANI and Mn-PANI, the first weight loss around 100 °C is observed due to the release of a small amount of water or volatile substances present in the electrode materials. The second weight loss at around 270 °C for both

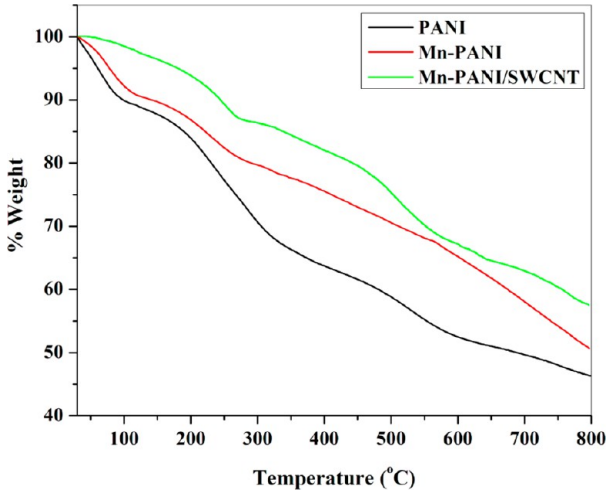

Figure 17. TGA thermograms of pure PANI, Mn-PANI, and Mn-PANI/SWCNT nanocomposites.

Mn-PANI and Mn-PANI/SWCNT nanocomposites is only because of the removal of dopant. There is common decomposition for all the electrode materials between 318 and 566 °C, corresponding to the decomposition of the backbone structure of PANI.[46] In Mn-PANI/SWCNT nanocomposites, an additional decomposition is observed between 580 and 740 °C because of the existence of a new PANI/SW phase.[47] So, from the TGA analysis, it is observed that the nanocomposite showed better thermal stability compared to PANI and Mn-PANI. The increase in the thermal stability for Mn-PANI/SWCNT nanocomposites is due to the presence of the SWCNTs in the composite, and also, there are strong $\pi-\pi$ interactions between PANI and SWCNTs. Additionally, the uniform coating of the Mn-doped PANI over SWCNTs

dx.doi.org/10.1021/sc5000072 | ACS Sustainable Chem. Eng. 2014, 2, 1114−1127

surfaces may be the possible reason for thermal stability. The weight loss at different temperatures for PANI, Mn-PANI, and Mn-PANI/SWCNT nanocomposites is given in Table 9.

Table 9. Thermal Stability Data for PANI, Mn-PANI, and Mn-PANI/SWCNT Nanocomposite Extracted from TGA Thermograms

	weight loss at temperature (%)			
sample	100 °C	300 °C	500 °C	700 °C
PANI	10.1	29.33	41.13	50.40
Mn-PANI	7.7	20.19	29.47	42.02
Mn-PANI/SWCNT	1.46	13.56	24.71	37.05

CONCLUSIONS

In conclusion, a simple *in situ* polymerization technique has been used for the synthesis of Mn-PANI/SWCNT nanocomposites. Spectroscopic techniques proved the interaction between Mn with PANI as well as PANI and SWCNTs. Morphological analysis confirmed the uniform coating of SWCNTs surfaces by Mn-doped PANI. The Mn-PANI/SWCNT nanocomposites exhibited the highest specific capacitance of 546 F/g at 0.5 A/g current density and retained their 88.13% specific capacitance over 1000 charge/discharge cycles. Both the transition metal (Mn^{2+}) as well as SWCNTs play a significant role for the increment of specific capacitance. The nanocomposites achieved maximum energy density of 194.13 Wh/kg at 0.5 A/g current density and also the highest power density of 2571.38 W/kg at 3 A/g current density. The transition metal doping improved the electrical conductivity, which is 9.65 S/cm for the nanocomposites. *I*−*V* characteristics confirmed the semiconducting nature of the electrode materials. The nanocomposites also exhibited highest thermal stability. Depending on superior electrochemical performance, the nanocomposites can be used as the electrode materials for supercapacitors.

AUTHOR INFORMATION

Corresponding Author

*E-mail: chapal12@yahoo.co.in. Tel: +91-3222-283978.

Notes

The authors declare no competing financial interest.

ACKNOWLEDGMENTS

The first author (S.D.) thanks Defence Research & Development Organization (DRDO), India, for financial support. P.B. and G.H. thank the Council of Scientific and Industrial Research (CSIR), New Delhi, India, for their financial support. The authors gratefully acknowledge Sandipta Roy, CRNTS, IIT Bombay, for Raman analysis. The authors are also thankful to IIT Kharagpur for instrumental facilities.

REFERENCES

(1) Simon, P.; Gogotsi, Y. Materials for electrochemical capacitors. *Nat. Mater.* **2008**, *7*, 845−854.
(2) Winter, M.; Brodd, R. J. What are batteries, fuel cells, and supercapacitors? *Chem. Rev.* **2004**, *104*, 4245−4269.
(3) Li, D.; R. Kaner, B. Shape and aggregation control of nanoparticles: Not shaken, not stirred. *J. Am. Chem. Soc.* **2006**, *128*, 968−675.
(4) Woo, S. W.; Dokko, K.; Nakano, H.; Kanamura, K. Incorporation of polyaniline into macropores of three-dimensionally ordered macroporous carbon electrode for electrochemical capacitors. *J. Power Sources* **2009**, *190*, 596−600.
(5) Palaniappan, S.; John, A.; Amarnath, C. A.; Rao, V. J. Mannich-type reaction in solvent free condition using reusable polyaniline catalyst. *J. Mol. Catal. A: Chem.* **2004**, *218*, 47−53.
(6) Sathiyanarayanan, S.; Jeyaprabha, C.; Venkatachari, G. Influence of metal cations on the inhibitive effect of polyaniline for iron in 0.5 M H_2SO_4. *Mater. Chem. Phys.* **2008**, *107*, 350−355.
(7) Liu, J.; Sun, J.; Gao, L. A promising way to enhance the electrochemical behavior of flexible single-walled carbon nanotube/polyaniline composite films. *J. Phys. Chem. C* **2010**, *114*, 19614−19620.
(8) Gupta, V.; Miura, N. Influence of the microstructure on the supercapacitive behavior of polyaniline/single-wall carbon nanotube composites. *J. Power Sources* **2006**, *157*, 616−620.
(9) Gupta, V.; Miura, N. Polyaniline/single-wall carbon nanotube (PANI/SWCNT) composites for high performance supercapacitors. *Electrochim. Acta* **2006**, *52*, 1721−1726.
(10) Abdiryim, T.; Ubul, A.; Jamal, R.; Rahman, A. Solid-state synthesis of polyaniline/single-walled carbon nanotubes: A comparative study with polyaniline/multiwalled carbon nanotubes. *Materials* **2012**, *5*, 1219−1231.
(11) Zhou, Y.; He, B.; Zhou, W.; Huang, J.; Li, X.; Wu, B.; Li, H. Electrochemical capacitance of well-coated single-walled carbon nanotube with polyaniline composites. *Electrochim. Acta* **2004**, *49*, 257−262.
(12) Zhou, Y.; He, B.; Zhou, W.; Li, H. Preparation and electrochemistry of SWNT/PANI composite films for electrochemical capacitors. *J. Electrochem. Soc.* **2004**, *151*, A1052−A1057.
(13) Huang, J.-E.; Li, X.-H.; Xu, J.-C.; Li, H.-L. Well-dispersed single-walled carbon nanotube /polyaniline composite films. *Carbon* **2003**, *41*, 2731−2736.
(14) Abdel-Fattah, T. M.; Ebrahim, S.; Soliman, M.; Hafez, M. Dye-sensitized solar cells based on polyaniline-single wall carbon nanotubes composite. *ECS J. Solid State Sci. Technol.* **2013**, *2*, M13−M16.
(15) Liu, J.; Sun, J.; Gao, L. Flexible single-walled carbon nanotubes/polyaniline composite films and their enhanced thermoelectric properties. *Nanoscale* **2011**, *3*, 3616−3619.
(16) Granot, E.; Basnar, B.; Cheglakov, Z.; Katz, E.; Willner, I. Enhanced bioelectrocatalysis using single-walled carbon nanotubes (SWCNTs)/polyaniline hybrid systems in thin-film and microrod structures associated with electrodes. *Electroanalysis* **2006**, *18*, 26−34.
(17) Ramamurthy, P. C.; Malshe, A. M.; Harrell, W. R.; Gregory, R. V.; McGuire, K.; Rao, A. M. Polyaniline/single-walled carbon nanotube composite electronic devices. *Solid-State Electron.* **2004**, *48*, 2019−2024.
(18) Dhand, C.; Solanki, P. R.; Dutta, M.; Malhotra, B. D. Polyaniline/single-walled carbon nanotubes composite based triglyceride biosensor. *Electroanalysis* **2010**, *22*, 2683−2693.
(19) Yan, C.; Zou, L.; Short, R. Single-walled carbon nanotubes and polyaniline composites for capacitive deionization. *Desalination* **2012**, *290*, 125−129.
(20) Mikhaylova, A. A.; Tusseeva, E. K.; Mayorova, N. A.; Rychagov, A. Y.; Volfkovich, Y. M.; Krestinin, A. V.; Khazova, O. A. Single-walled carbon nanotubes and their composites with polyaniline. Structure, catalytic and capacitive properties as applied to fuel cells and supercapacitors. *Electrochim. Acta* **2011**, *56*, 3656−3665.
(21) Patil, D. S.; Shaikh, J. S.; Dalavi, D. S.; Karanjkar, M. M.; Devan, R. S.; Ma, Y. R.; Patil, P. S. An Mn doped polyaniline electrode for electrochemical supercapacitor. *J. Electrochem. Soc.* **2011**, *158*, A653−A657.
(22) Dhibar, S.; Sahoo, S.; Das, C. K.; Singh, R. Investigation on copper chloride doped polyaniline composites as efficient electrode materials for supercapacitor applications. *J. Mater. Sci: Mater. Electron.* **2013**, *24*, 576−585.
(23) Qian, T.; Zhou, X.; Yu, C.; Wu, S.; S, J. Highly dispersed carbon nanotubes/polypyrrole core/shell composites with improved electrochemical capacitive performance. *J. Mater. Chem. A* **2013**, *1*, 15230−15234.

(24) Wei, Y.; Kong, L.-T.; Yang, R.; Wang, L.; Liu, J.-H.; Huang, X.-J. Electrochemical impedance determination of polychlorinated biphenyl using a pyrenecyclodextrin-decorated single-walled carbon nanotube hybrid. *Chem. Commun.* **2011**, *47*, 5340−5342.
(25) Shul, G.; Ruiz, C. A. C.; Rochefort, D.; Brooksbly, P. A.; Belanger, D. Electrochemical functionalization of glassy carbon electrode by reduction of diazonium cation in protic ionic liquid. *Electrochim. Acta* **2013**, *106*, 378−385.
(26) Zhang, Y.; Chi, Y.; Su, S. Determination of dopamine in the presence of ascorbic acid by poly(styrene sulfonic acid) sodium salt/single-wall carbon nanotubes film modified glassy carbon electrode. *Anal. Biochem.* **2006**, *350*, 285−291.
(27) Planes, G. A.; Rodríguez, J. L.; Miras, M. C.; García, G.; Pastor, E.; Barbero, C. A. Spectroscopic evidence for intermediate species formed during aniline polymerization and polyaniline degradation. *Phys. Chem. Chem. Phys.* **2010**, *12*, 10584−10593.
(28) Neoh, K. G.; Tang, E.; Tan, K. L. Co-existence of external protonation and self-doping in polyaniline. *Synth. Met.* **1993**, *60*, 13−21.
(29) Ginic-Markovic, M.; Matisons, J. G.; Cervini, R.; Simon, G. P.; Fredericks, P. M. Synthesis of new polyaniline/nanotube composites using ultrasonically initiated emulsion polymerization. *Chem. Mater.* **2006**, *18*, 6258−6265.
(30) Jeon, I.-Y.; Kang, S.-W.; Tan, L.-S.; Baek, J.-B. Grafting of polyaniline onto the surface of 4-aminobenzoyl-functionalized multi-walled carbon nanotube and its electrochemical properties. *J. Polymer Sci., Part A: Polymer Chem.* **2010**, *48*, 3103−3112.
(31) Ubul, A.; Jamal, R.; Rahman, A.; Awut, T.; Nurulla, I.; Abdiryim, T. Solid-state synthesis and characterization of polyaniline/multi-walled carbon nanotubes composite. *Synth. Met.* **2011**, *161*, 2097−2102.
(32) Reddy, K. R.; Sin, B. C.; Yoo, C. H.; Sohn, D.; Lee, Y. Coating of multiwalled carbon nanotubes with polymer nanospheres through microemulsion polymerization. *J. Colloid Interface Sci.* **2009**, *340*, 160−165.
(33) Pal, M.; Hirota, K.; Sakata, H. Electrical and optical properties of as-deposited V_2O_5-TeO_2 amorphous films and their annealing effects. *Phys. Status Solidi A* **2003**, *196*, 396−404.
(34) Huang, L. M.; Wen, T. C.; Gopalan, A.; Ren, F. Structural influence on the electronic properties of methoxy substitute polyaniline/aluminum Schottky barrier diodes. *Mater. Sci. Eng., B* **2003**, *104*, 88−95.
(35) Wei, Z.; Wan, M.; Lin, T.; Dai, L. Polyaniline nanotubes doped with sulfonated carbon nanotubes made via self-assembly process. *Adv. Mater.* **2003**, *15*, 136−139.
(36) Yuan, B.; Yu, L.; Sheng, L.; An, K.; Zhao, X. Comparison of electromagnetic interference shielding properties between single-wall carbon nanotube and graphene sheet/polyaniline composites. *J. Phys. D: Appl. Phys.* **2010**, *45*, 235108−235114.
(37) Yan, J.; Wei, T.; Fan, Z.; Qian, W.; Zhang, M.; Shen, X.; Wei, F. Preparation of graphene nanosheet/carbon nanotubes/polyaniline composite as electrode materials for supercapacitors. *J. Power Sources* **2010**, *195*, 3041−3045.
(38) Tawansi, A.; El-khodary, A.; Zidan, H. M.; Badr, S. I. The effect of $MnCl_2$ filler on the optical window and the physical properties of PMMA films. *Polym. Test.* **2002**, *21*, 381−387.
(39) Chew, S. Y.; Ng, S. H.; Wang, J.; Novak, P.; Krumeich, F.; Chou, S. L.; Chen, J.; Liu, H. K. Flexible free-standing carbon nanotubes films for model lithium-ion batteries. *Crabon* **2009**, *47*, 2976−2983.
(40) Giri, S.; Ghosh, D.; Das, C. K. In situ synthesis of cobalt doped polyaniline modified graphene composite for high performance supercapacitor electrode materials. *J. Electroanal. Chem.* **2013**, *697*, 32−45.
(41) Grinou, A.; Bak, H.; Yun, Y. S.; Jin, H.-J. Polyaniline/silver nanoparticle-doped multiwalled carbon nanotube composites. *J. Dispersion Sci. Technol.* **2012**, *33*, 750−755.
(42) Dhibar, S.; Sahoo, S.; Das, C. K. Copper chloride doped polyaniline/multiwalled carbon nanotubes nanocomposites: superior electrode materials for supercapacitor applications. *Polym. Compos.* **2013**, *34*, 512−525.
(43) Zhang, J.; Kong, L. B.; Wang, B.; Luo, Y. C. In-situ electrochemical polymerization of multi-walled carbon nanotubes/polyaniline composites films for electrochemical supercapacitors. *Synth. Met.* **2009**, *159*, 260−266.
(44) Li, G.-R.; Feng, Z.-P.; Zhong, J.-H.; Wang, Z.-L.; Tong, Y.-X. Electrochemical synthesis of polyaniline nanobelts with predominant electrochemical performances. *Macromolecules* **2010**, *43*, 2178−2183.
(45) Li, X.; Wu, B.; Huang, J.; Zhang, J.; Liu, Z.; Li, H. Fabrication and characterization of well-dispersed single-walled carbon nanotube /polyaniline composites. *Carbon* **2002**, *411*, 1645−1687.
(46) Rodrigues, P. C.; De Souza, G. P.; Motta, N. D.; Joaquim, D.; Akcelrud, L. Thermal treatment and dynamic mechanical thermal properties of polyaniline. *Polymer* **2002**, *43*, 5493−5499.
(47) Sainz, R.; Benito, A. M.; Martinez, M. T.; Galindo, J. F.; Sotres, J.; Baro, A. M.; Master, W. K. Soluble self-aligned carbon nanotubes/polyaniline composites. *Adv. Mater.* **2005**, *17*, 278−281.